ARL-TR-7795 ● SEP 2016

US Army Research Laboratory

Evaluation of the US Army Research Laboratory Squeeze 5 Magnetic Flux Compression Generator

by Peter Bartkowski, Paul Berning, and Seth Halsey

NOTICES

Disclaimers

The findings in this report are not to be construed as an official Department of the Army position unless so designated by other authorized documents.

Citation of manufacturer's or trade names does not constitute an official endorsement or approval of the use thereof.

Destroy this report when it is no longer needed. Do not return it to the originator.

ARL-TR-7795 ● SEP 2016

US Army Research Laboratory

Evaluation of the US Army Research Laboratory Squeeze 5 Magnetic Flux Compression Generator

by Peter Bartkowski, Paul Berning, and Seth Halsey
Weapons and Materials Research Directorate, ARL

REPORT DOCUMENTATION PAGE

Form Approved
OMB No. 0704-0188

1. REPORT DATE *(DD-MM-YYYY)*	2. REPORT TYPE	3. DATES COVERED (From - To)
September 2016	Technical Report	1 October 2013–30 September 2016

4. TITLE AND SUBTITLE
Evaluation of the US Army Research Laboratory Squeeze 5 Magnetic Flux Compression Generator

5a. CONTRACT NUMBER

5b. GRANT NUMBER

5c. PROGRAM ELEMENT NUMBER

6. AUTHOR(S)
Peter Bartkowski, Paul Berning, and Seth Halsey

5d. PROJECT NUMBER
AH80

5e. TASK NUMBER

5f. WORK UNIT NUMBER

7. PERFORMING ORGANIZATION NAME(S) AND ADDRESS(ES)
US Army Research Laboratory
ATTN: RDRL-WMP-E
Aberdeen Proving Ground, MD 21005-5066

8. PERFORMING ORGANIZATION REPORT NUMBER
ARL-TR-7795

9. SPONSORING/MONITORING AGENCY NAME(S) AND ADDRESS(ES)

10. SPONSOR/MONITOR'S ACRONYM(S)

11. SPONSOR/MONITOR'S REPORT NUMBER(S)

12. DISTRIBUTION/AVAILABILITY STATEMENT
Approved for public release; distribution is unlimited.

13. SUPPLEMENTARY NOTES

14. ABSTRACT
The US Army Research Laboratory has a program to develop a Magnetic Flux Compression device capable of generating a 2 mega-ampere peak output current. This report details the experimental results of the Squeeze 5 device. The objective was to improve the output current and operating efficiency over the previous Squeeze 4 device. Several different loss mechanisms were evaluated, such as magnetic field diffusion, armature cracking, high-voltage insulation, and electrical arcing.

15. SUBJECT TERMS
magnetic flux compression, field diffusion, mega ampere, high voltage, flux loss

16. SECURITY CLASSIFICATION OF:			17. LIMITATION OF ABSTRACT	18. NUMBER OF PAGES	19a. NAME OF RESPONSIBLE PERSON
a. REPORT	b. ABSTRACT	c. THIS PAGE			Peter Bartkowski
Unclassified	Unclassified	Unclassified	UU	26	19b. TELEPHONE NUMBER (Include area code) 410-278-0210

Contents

List of Figures iv

List of Tables iv

1. Introduction 1

2. Magnetic Flux Compression Theory 1

3. Flux Compression Losses 1

4. Design of the Squeeze 5 2

5. Armature Expansion Experiments 5

6. Experimental Data 9

7. Conclusions 13

8. References 14

Appendix. Armature Expansion Images 15

List of Symbols, Abbreviations, and Acronyms 19

Distribution List 20

List of Figures

Fig. 1 Cross section of coaxial MFC 2

Fig. 2 Cross section of the base Squeeze 5 coaxial MFC 3

Fig. 3 Cross section of the Squeeze 5 coaxial MFC with output glide plane and high-pressure (HP) contacts 3

Fig. 4 a) Cross-sectional view without and b) with armature cracks 4

Fig. 5 Cross section of the Squeeze 5 coaxial MFC with output glide plane and HP contacts 5

Fig. 6 Cross-sectional view of high-pressure contacts 5

Fig. 7 Armature expansion experimental setup 6

Fig. 8 Comparison of armature performances at 20-µs time after detonation 7

Fig. 9 Comparison of armature performances at 40-µs time after detonation 8

Fig. 10 Comparison of armature PVC insulation at 20- and 40-µs time after detonation 9

Fig. 11 MFC output current using 6063-TO, T6 armatures and aluminum (Al) vs. stainless steel (SS) loads 11

Fig. 12 MFC output current comparison between coil insulations 12

Fig. 13 MFC output current comparison with output glide plane and HP contacts 12

Fig. A-1 Experiment A 16

Fig. A-2 Experiment B 16

Fig. A-3 Experiment C 17

Fig. A-4 Experiment D 17

Fig. A-5 Experiment E 18

List of Tables

Table 1 Summary of armature expansion experiments 6

Table 2 Summary of MFC experiments 10

1. Introduction

The US Army Research Laboratory (ARL) has an active program to develop a Magnetic Flux Compression (MFC) device capable of producing 2 mega-amps of current into a low-impedance load. Previous evaluation[1] of MFC devices at ARL resulted in a device design capable of producing just more than one mega-ampere of current with a figure of merit between 0.56 and 0.72.[1] Low figures of merit clearly indicate losses in the systems, which are significantly reducing output current and energy. This report describes an effort to determine the source of these losses and associated attempts to mitigate them.

Changes were made to some system components to determine the effect on output and figure of merit. Experiments were also conducted to evaluate the material properties of the aluminum armatures under explosive expansion.

2. Magnetic Flux Compression Theory

Conductors that move through or compress a magnetic field perform work. This work increases the energy in the system. This mechanical energy is transferred to the parts of the electrical system that are coupled to the magnetic field. In an explosive MFC, a conductor is propelled using explosives to compress a magnetic field. The result is an increase in current conducting through that conductor. A typical MFC will use a seed current to generate the initial seed magnetic field within a shielded enclosure. Then an explosive charge is detonated, decreasing the volume of the shielded enclosure. This decrease in volume increases the strength of the magnetic field. As a result, an electrical load connected to the MFC will see an increase or magnification of the initial seed current. Some MFCs are capable of magnifying the seed current by a factor of several hundred. A relatively small initial seed current can be amplified into a much larger pulsed current.

3. Flux Compression Losses

The extreme voltages, currents, and magnetic fields within a functioning MFC device push the devices and their materials to their limits. At these limits, material properties such as resistivity become highly nonlinear, greatly increasing losses in the system. Fowler et al.[2] suggest that this limit is on the order of 1 mega-ampere of current per centimeter of conductor width; he did not identify this limit with respect to a specific conductor material. The sharp closing angle the expanding armature makes with the coil (as seen in Fig. 1) and the high rate of change of

current combine to create extremely high electric fields between the armature and coil. This can lead to premature breakdown of insulation and can result in arcing that robs energy from the system. Magnetic field diffusion into the conducting portions of the system can also play a role. The magnetic field sets up initially on the internal surface of the coil and external surface of the armature, and then diffuses into these materials with time. Any magnetic energy trapped within the conducting material cannot be compressed, and thus is lost energy in the system. Even worse, if the armature material begins to prematurely fail, the shielding effect required to compress the magnetic field is lost and the magnetic field leaks into the interior volume of the armature. Any field that leaks into the interior volume of the armature will not be compressed and is therefore lost to the device. To investigate the effects of nonlinearity and lost magnetic flux due to magnetic field diffusion, a new device—the "Squeeze 5"—was designed.

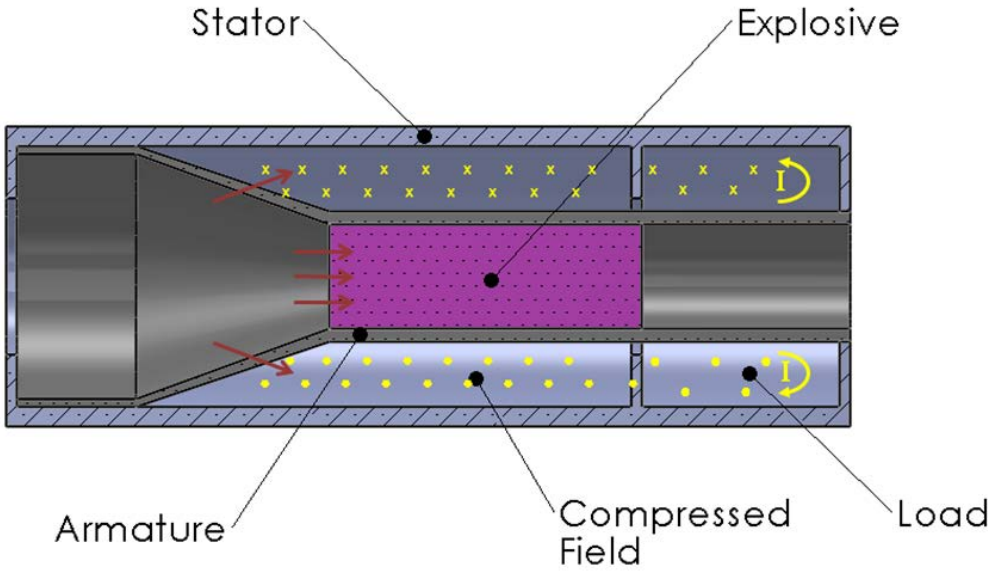

Fig. 1 Cross section of coaxial MFC

4. Design of the Squeeze 5

The Squeeze 5 device, shown in Figs. 2 and 3, is similar to the Squeeze 4 design[1] but with several design changes. To reduce nonlinear effects, the coil was changed from aluminum to copper. The coil was machined from C12200 copper alloy tube. Both aluminum and copper increase in resistivity as the conductors increase in temperature due to ohmic heating. This can quickly lead to a runaway condition where the temperature and resistance of the conductors become nonlinear and rise very quickly. Switching the coil material reduced the resistivity from 33×10^{-9} Ω-m of the 6063-T6 aluminum[3] to 20.3×10^{-9} Ω-m for the C12200

copper.[4] The volumetric heat capacity of copper (3.43 J/cc K)[4] is also higher than that of aluminum (2.42 J/cc K).[5] These 2 factors should reduce the temperature increase in the conductors, resulting in a lower resistance, higher output currents, and improved efficiency.

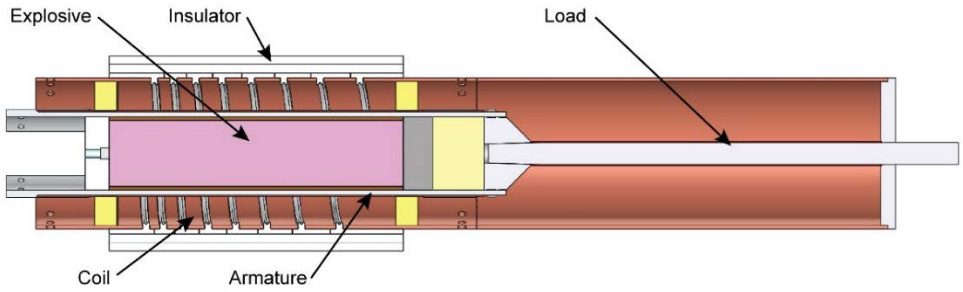

Fig. 2 Cross section of the base Squeeze 5 coaxial MFC

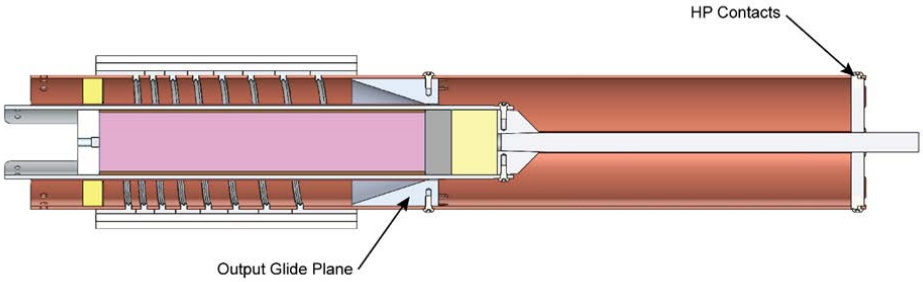

Fig. 3 Cross section of the Squeeze 5 coaxial MFC with output glide plane and high-pressure (HP) contacts

To reduce the lost flux from magnetic field diffusion, the copper coil outer diameter was increased to 5.125 inches (instead of 4.50-inch aluminum). This increased the magnetic volume by 45%. To keep the magnetic energy constant, the number of coil turns was decreased from 9 to 7, reducing the magnetic field strength generated. In theory, any field that diffuses into the materials would be weaker in strength, decreasing the amount of energy lost due to incompressible magnetic flux. Reducing the number of turns in the coil also has the benefit of increasing the final output width of the conductors from 20 to 29 mm. This reduces current density and resistance, yielding lower heating, higher currents, and greater efficiency.

The armatures were the same as in the Squeeze 4 design[1] except that they were made from 2 different materials to investigate the effect of cracking during expansion. Neuber's research[6] suggests that annealing of armatures can improve MFC performance. Some of the 6063-T6 armatures were annealed to the O temper (TO) state in an effort to reduce fracture. The armature must shield the magnetic

flux from penetrating into the interior volume to compress the flux. The actual shielding is not by the metal itself, but caused by induced eddy currents that flow circumferentially around the armature (Fig. 4a). The eddy currents generate a countermagnetic field that pushes on the magnetic field in between the armature and coil, compressing it. Any cracks forming on the armature exterior during expansion will interfere with the flow of the eddy currents (which are initially flowing on the exterior armature surface, prior to field diffusion). This will manifest itself through an increase of resistance, allowing the magnetic field to very rapidly diffuse into the interior of the armature (Fig. 4b), losing the ability to compress the magnetic flux. If cracks are a problem, annealing the material may help reduce fracture and reduce lost flux.

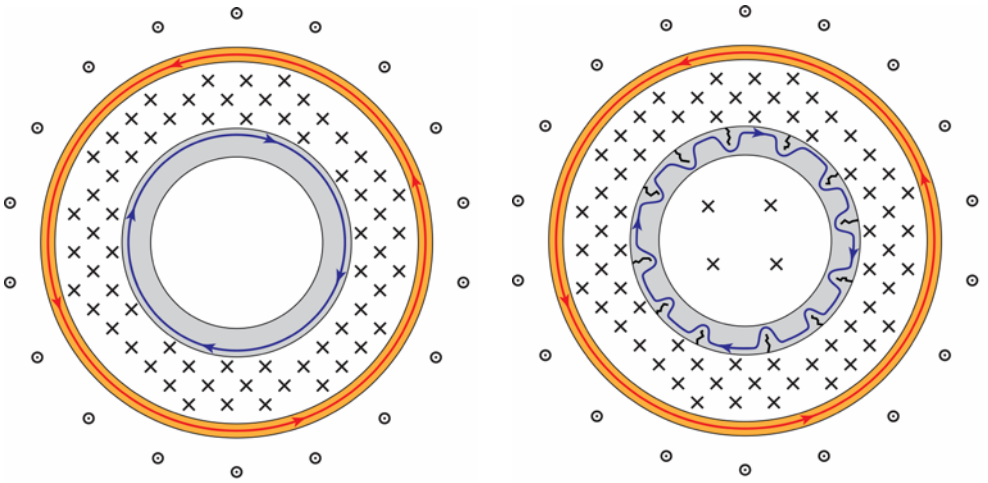

Fig. 4 a) Cross-sectional view without and b) with armature cracks

To investigate arcing between the coil and expanding armature as a source of losses, one MFC device was fabricated with additional insulation on the inside of the coil. In the base device, the only insulation is a coating of PVC heat shrink tubing applied to the exterior of the armature. This PVC must evenly stretch with the expanding armature to reduce internal arcing in front of the contact point. A dual layer of 0.25-mm-thick polyester film was inserted in between the armature and coil to provide additional insulation.

Another potential loss in the system is the load itself. Arcing between connecting parts of the load can result in a large increase in resistance. This may decrease output current during compression, but will become increasingly noticeable as a rapid decrease in output current after the compression has ended. A second modified device (Fig. 5) was designed and built to reduce the possibility of arcing in the load section. It included an output glide plane and high-pressure contacts between the load tube and return endcap. The output glide plane was machined

from 6063-T6 aluminum to an internal angle of 18.0°. Eight 1/4-inch-diameter bolts were used to attach it to the tube at the end of the coil. The high-pressure contacts (Fig. 6) were created by machining a 0.30-inch-wide groove, 0.030-inches-deep, along the center of the edge of the 0.50-inch-thick endcap. Eight 1/4-inch-diameter bolts were used to attach it to the end of the load tube.

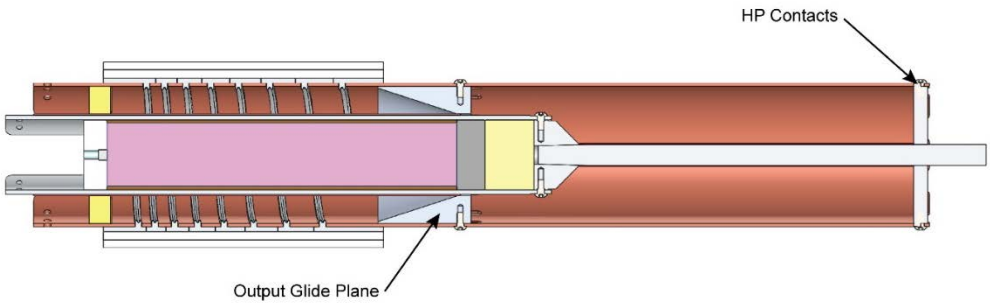

Fig. 5 Cross section of the Squeeze 5 coaxial MFC with output glide plane and HP contacts

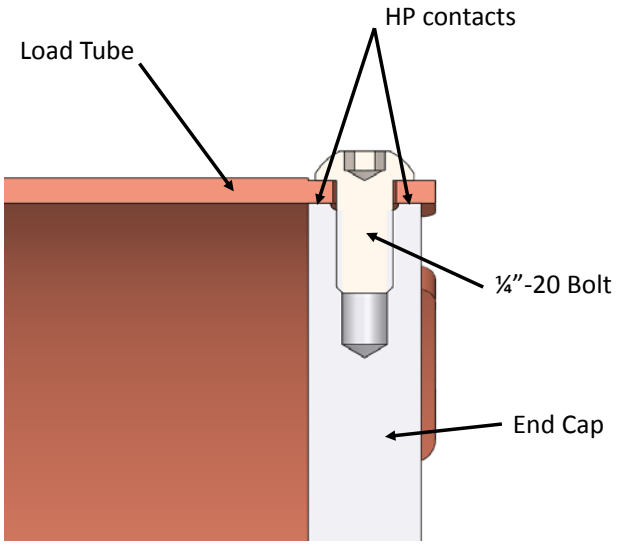

Fig. 6 Cross-sectional view of high-pressure contacts

5. Armature Expansion Experiments

To investigate the possibility of armature cracking being an issue, an experimental series was devised to look for cracking of the armatures during expansion. Armatures were filled with the Comp-B explosive charge and detonated. During the explosive expansion, a Sim-8 Framing Camera, manufactured by Specialized Imaging, was used to take 8 image-intensified photos at 150-ns exposure time. The

first image was taken at 15 µs after detonation and the next 7 images were captured at 5-µs intervals. Lighting was supplied by 4 Mega Flash PF300 flashbulbs on each end of the armature. As seen in Fig. 7, the light was reflected by aluminum foil inside a plywood cover to evenly illuminate the armature. In addition, a turning mirror was used to protect the camera from the radial fragments produced by the expanding armature.

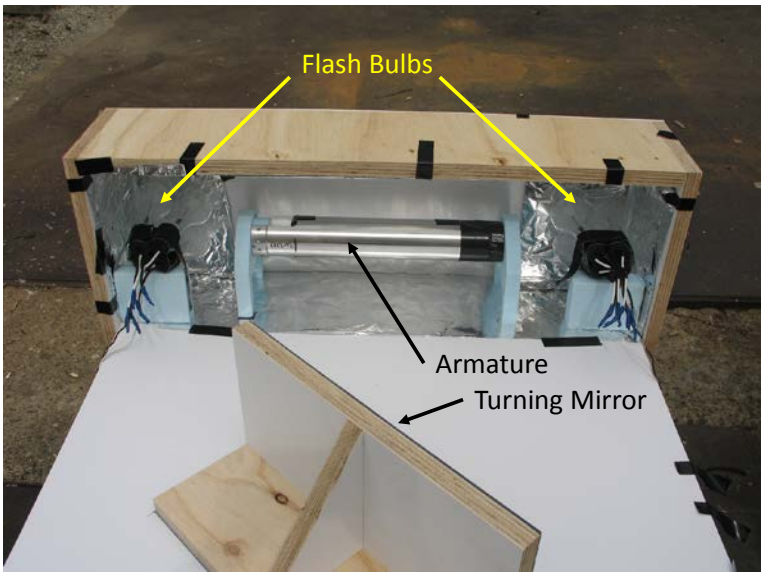

Fig. 7 Armature expansion experimental setup

Four experiments (A–D) were conducted on a combination of aluminum tempers and wall thicknesses. The final Experiment E was also conducted to look at the stretching of the PVC insulation placed on the armature. Table 1 summarizes the experiments conducted. All of the images captured during armature expansion experiments can be found in the Appendix.

Table 1 Summary of armature expansion experiments

Experiment	6063 temper	Wall thickness (inches)	PVC insulation?
A	T6	0.25	No
B	T6	0.16	No
C	TO	0.25	No
D	TO	0.16	No
E	TO	0.25	Yes

Experiments A and C used a 0.25-inch-thick wall 6063 aluminum armature tube. Experiment A was the original T6 temper and Experiment C was the annealed TO temper. The T6 temper tube shows surface cracks forming as early as 20 µs after

detonation (Fig. 8). The cracks grow in length with time as the tube expands. At 30-μs time a hot spot appears, which indicates a full depth crack has formed, letting the detonation products escape. More of these full depth cracks form with time resulting in a fully compromised tube by 45 μs. The annealed TO temper tube shows much better performance. Although small surface cracking can be seen at 25 μs at the bell end of the expansion, they do not grow in length. The rest of the expanding armature has a smooth outer texture as it expands. Only at 50-μs time do we see any indication of through cracks forming at the very edge of the bell end of the expansion.

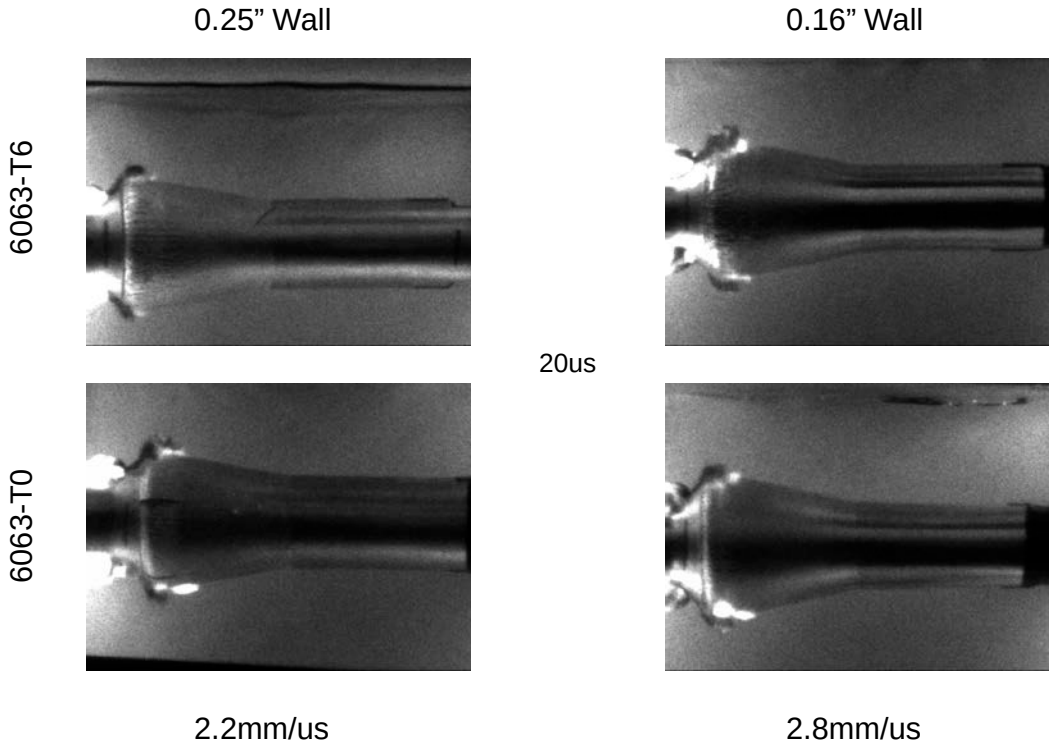

Fig. 8 Comparison of armature performances at 20-μs time after detonation

Experiments B and D used a thinner 0.16-inch-thick wall 6063 aluminum armature tube. Experiment B was the original T6 temper and Experiment D was the annealed TO temper. As in Experiment A, the T6 temper tube shows surface cracks forming as early as 20 μs after detonation and the cracks grow in length with time as the tube expands. At 25-μs time, hot spots appear that indicate full depth cracks have formed at the bell end of the expansion. More of these full depth cracks quickly form with time resulting in a fully compromised tube by 35 μs. The annealed TO temper tube shows much better performance. Although small surface cracking can be seen at 20 μs at the bell end of the expansion, they grow very little in length. The rest of the expanding armature has a relatively smooth outer texture as it expands.

Only at 40-µs time do we see any indication of through cracks forming at the very edge of the bell end of the expansion.

Considering that the armatures only need to conduct current as they expand until they impact the outer coil, we can discount the condition of the bell end of the expansion at late times. Initial impact would have occurred at approximately 20-µs time for the Squeeze 4 device and 22-µs time for the Squeeze 5 device. However, the late time images are a good comparison tool. The defects start early, then grow and become amplified with time. Even surface imperfections can have a significant impact on the flow of eddy currents as they initially start on this outer surface and take time to diffuse inward. Figure 9 shows a comparison of Experiments A–D at 40-µs time. As is clearly evident, the TO temper tubes appear to have much better late time performance. This suggests that they also have a smoother outer surface at early times of expansion, which may result in better shielding and compression of the magnetic flux between the armature and coil.

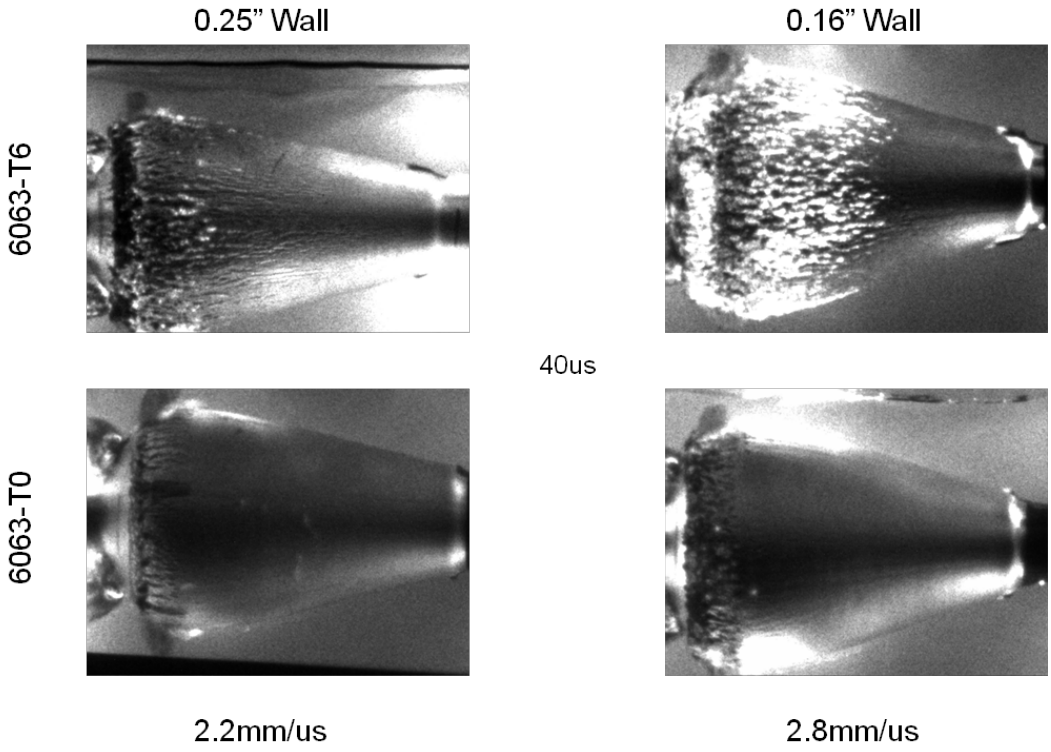

Fig. 9 Comparison of armature performances at 40-µs time after detonation

Experiment E was conducted with a 0.25-inch-thick wall armature of TO temper covered in PVC heat shrink tubing. The goal was to observe the insulation for failure indications. The internal working voltage of this device is approximately 50 kV. To prevent internal arcing, it is necessary for the insulation to hold off this

high voltage as the armature expands toward the coil. Figure 10 shows images of the armature insulation at 20- and 40-μs time after detonation. The insulation appears to be intact as it is expanding with no gross failures. However, we cannot determine the actual insulation thickness. The thickness does not appear to be constant, some axial striations are present. These are most likely due to slight thickness variations created during the extrusion process in manufacturing, which are then accentuated by the rapid expansion after detonation.

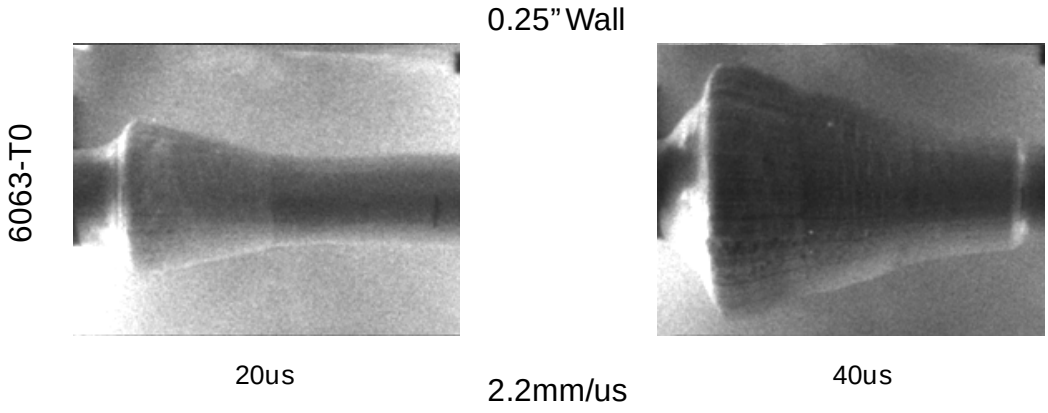

Fig. 10 Comparison of armature PVC insulation at 20- and 40-μs time after detonation

6. Experimental Data

To evaluate the effect of armature annealing on flux compressor performance, a series of experiments were performed with armatures made from 6063-T6 aluminum and the same aluminum annealed to the 6063-TO temper. Three other changes were also evaluated. Two experiments were performed to evaluate the effect of an increased load resistance by replacing the aluminum return rod in the center of the load with a stainless steel one. One experiment was conducted to evaluate the effect of increasing the insulation inside the coil. Most flux compression experiments to date have also displayed a rapid decrease of current after the compression occurs, which is indicative of a fast increase in resistance of the load. This may be due to arcing between mating conductors. One experiment was conducted that incorporated an output glide plane and high-pressure contacts on the endcap in an effort to reduce arcing.

As in the previous Squeeze 4 experimental series,[1] data was collected on an Agilent DSO6000 series digital oscilloscope. The data consisted of timing signals for the switch and detonator initiation and current derivative (dI/dt) signals from calibrated Rogowski coils. Two Rogowski coils were used, one on the capacitor bank to measure the seed current, the other inside the load to measure load current. After

the experiment, the dI/dt signals are digitally integrated to yield the current versus time profiles.

The seed current was provided by a 535-μf capacitor bank. The initial charge voltage for all experiments was 10 kV. A high-voltage switch was used to initiate current flow from the capacitor bank and there was a delay of 44 μs before the detonator was initiated in the Composition-B explosive-filled armature.

In all, 8 experiments were conducted using this flux compressor design. A summary of the experiments is given in Table 2. The table includes the initial seed capacitor bank charge voltage, measured seed current, measured output current, calculated magnification factor, and the calculated figure of merit.[1] Experiments 10 and 13 failed to produce any meaningful results. The data from Experiment 10 indicates a short circuit occurred internally to the device, most likely due to damaged insulation during construction. The high-voltage switch failed to conduct when initiated in Experiment 13, resulting in no magnetic field to compress.

Table 2 Summary of MFC experiments

Experiment no.	Charge voltage (kV)	Peak seed current (kA)	Peak output current (kA)	Current mag. factor	Figure of merit (β)	Notes
10	10	Internal short circuit				0.16-inch-thick 6063-T6 armature aluminum load rod
11	10	94	750	7.96	0.67	0.16-inch-thick 6063-T6 armature stainless steel load rod
12	10	108	974	9.02	0.75	0.16-inch-thick 6063-TO armature aluminum load rod
13	10	Switch failed to fire				0.16-inch-thick 6063-TO armature stainless steel load rod
14	10	105	947	9.01	0.75	0.16-inch-thick 6063-T6 armature aluminum load rod
15	10	105	912	8.69	0.75	0.16-inch-thick 6063-T6 armature aluminum load rod extra coil insulation
16	10	100	790	7.90	0.68	0.16-inch-thick 6063-TO armature stainless steel load rod
17	10	107	982	9.18	0.76	0.16-inch-thick 6063-TO armature aluminum load rod output glide plane HP contacts on endcap

The effect of using annealed aluminum for the expanding armatures can be seen in Fig. 11. Experiments 12 and 14 both used an aluminum load rod; Experiment 12 used a TO temper aluminum armature, while Experiment 14 used a T6 temper. Experiments 16 and 11 both used a stainless steel load rod; Experiment 16 used a TO temper aluminum armature, while Experiment 11 used a T6 temper. The stainless steel had a nominal resistivity[7] of 740×10^{-9} Ω-m, while the aluminum[3] was 33×10^{-9} Ω-m. As we expected from the armature expansion experiments, both TO temper armatures produced higher outputs than the T6 tempers. However, the increase in peak current output was only approximately 3%. The 80% increase in resistance of the stainless steel load rod over the aluminum, decreased the peak generator output current by approximately 20%.

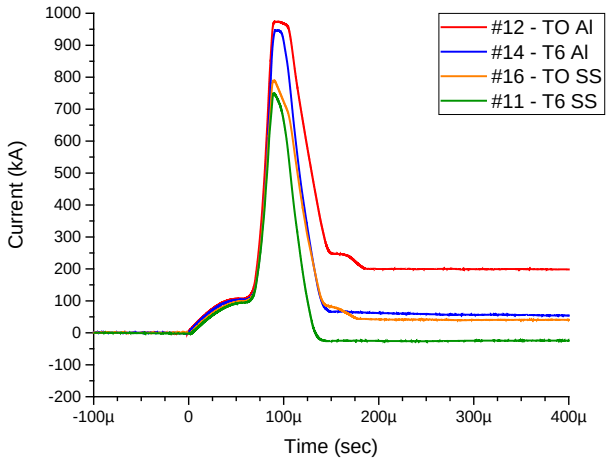

Fig. 11 MFC output current using 6063-TO, T6 armatures and aluminum (Al) vs. stainless steel (SS) loads

The internal working voltage of the flux compressor is estimated to be approximately 50 kV. Having adequate insulation is critical to device performance. To validate whether insulating the armature alone is sufficient to prevent arcing, additional insulation was added to Experiment 15. Two layers of 0.25-mm polyester film were added to the inside of the device between the armature and coil. Figure 12 compares the result from Experiment 15 to 14, which did not have the extra insulation. The extra insulation decreased output by 3.7%.

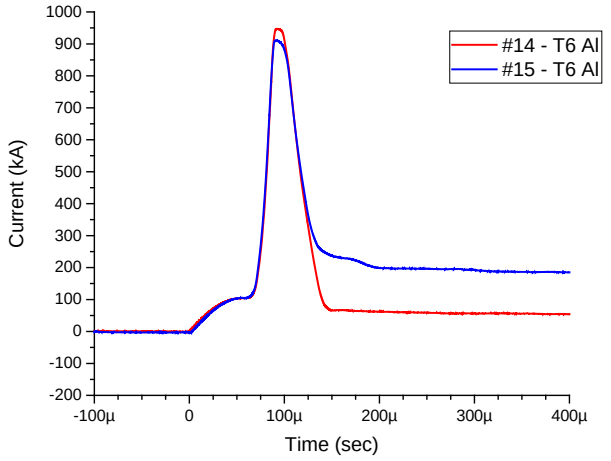

Fig. 12 MFC output current comparison between coil insulations

In an effort to decrease potential arcing inside the compression region and load, 2 modifications were made in Experiment 17. An output glide plane was added to the compression region to help trap flux and prevent conductors from separating. High-pressure contacts were also added to the return cap on the end of the load. This experiment used an annealed armature and aluminum load rod. A comparison of this experiment to Experiment 12 can be seen in Fig. 13. The modification clearly had a large impact on flow of current after the compression was complete. All previous experiments had a very fast drop in current shortly after compression, indicating a very fast rise in resistance. Experiment 17 however shows a sustained high current, indicating a much lower and nearly constant resistance of only 0.20 mΩ.

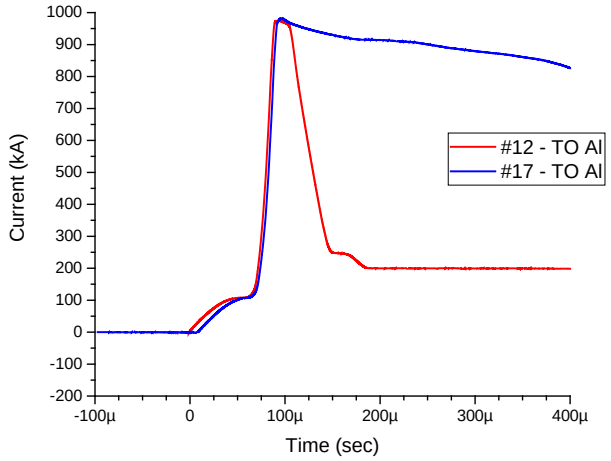

Fig. 13 MFC output current comparison with output glide plane and HP contacts

7. Conclusions

The 3 MFC devices used in Experiments 12, 14, and 15 produced nearly identical results. Even though the peak output currents for these experiments were different, the calculated figures of merit for these 3 trials were identical at 0.75. Differences in peak output current are attributable to slightly different seed currents and initial coil inductances. There did not appear to be a significant benefit to annealing the armatures. The amount of cracking of the armature at an expansion ratio of 1.74 was not enough to effect output current. There also did not appear to be a benefit to increasing the insulation between the coil and armature. This indicates that the PVC insulation on the armature is sufficient for this device. These 2 results may be different if a larger-diameter coil is used, which would increase the armature expansion ratio.

Experiment 17 produced the most interesting results. Adding the output glide plane and high-pressure contacts to the end cap resulted in a sustained high current. The previous experiments showed a rapid drop in current after compression ended, most likely due to contact separation and subsequent arcing. While the high magnetic forces will try to separate mated conductors, the inductance in the circuit will keep the current flowing by producing an arc. As the conductors continue to separate, the arcs will increase the voltage drop across these connections, rapidly dissipating the current. The output glide plane provides a bearing surface to arrest expansion of the armature, preventing the armature and tube at the end of the coil from separating. The high-pressure contacts between the load tube and the return end cap prevents arcing and holds the conductors together. These 2 features will be incorporated into all future devices.

Future work will investigate this device's ability to operate at higher currents. Previous experiments of the ARL Squeeze 4 device[1] showed a large drop in efficiency when operating with a larger seed current. The hope is that the larger output conductor width of this new device will reduce the current density and operate at a higher efficiency with a larger seed current.

8. References

1. Bartkowski P. Design and testing of the ARL Squeeze 4 helical flux compression generator. Aberdeen Proving Ground (MD): Army Research Laboratory (US); 2013 June. Report No.: ARL-TR-6477.

2. Fowler CM, Caird RS, Garn WB. An introduction to explosive magnetic flux compression generators. Los Alamos (NM): Los Alamos Scientific Laboratory (US); 1975. Report No.: LA-5.

3. ASM Aerospace Specification Metals Inc., Aluminum 6063-T6 [accessed 2016 Aug 12] http://asm.matweb.com/search/SpecificMaterial.asp?bassnum=MA6063T6.

4. Olin Brass World-Class Metals, C12200 (ASTM B152) Alloy Data Specifications [accessed 2016 Aug 12] http://www.olinbrass.com/resources/alloy-data-specifications/C12200-(ASTM B152).

5. Hodgman C, editor. Handbook of chemistry and physics. 44th ed. Cleveland (OH): The Chemical Rubber Publishing Co; 1962. p. 2352–2353.

6. Neuber AA. Explosively driven pulsed power. New York (NY): Springer; 2005.

7. ASM Aerospace Specification Metals Inc., AISI Type 316 Stainless Steel [accessed 2016 Aug 12] http://asm.matweb.com/search/SpecificMaterial.asp?bassnum=MQ316A.

Appendix. Armature Expansion Images

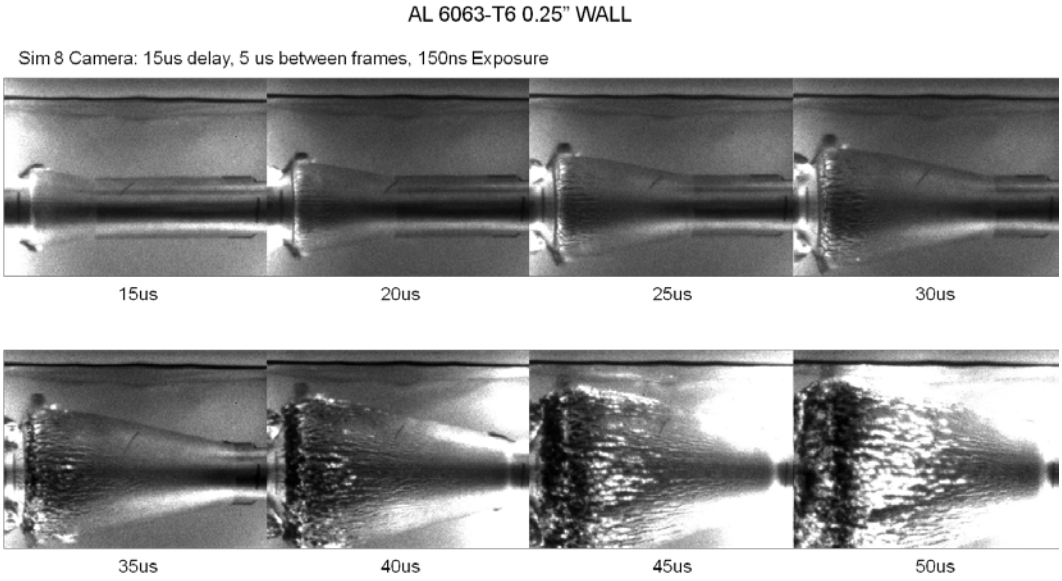

Fig. A-1 Experiment A

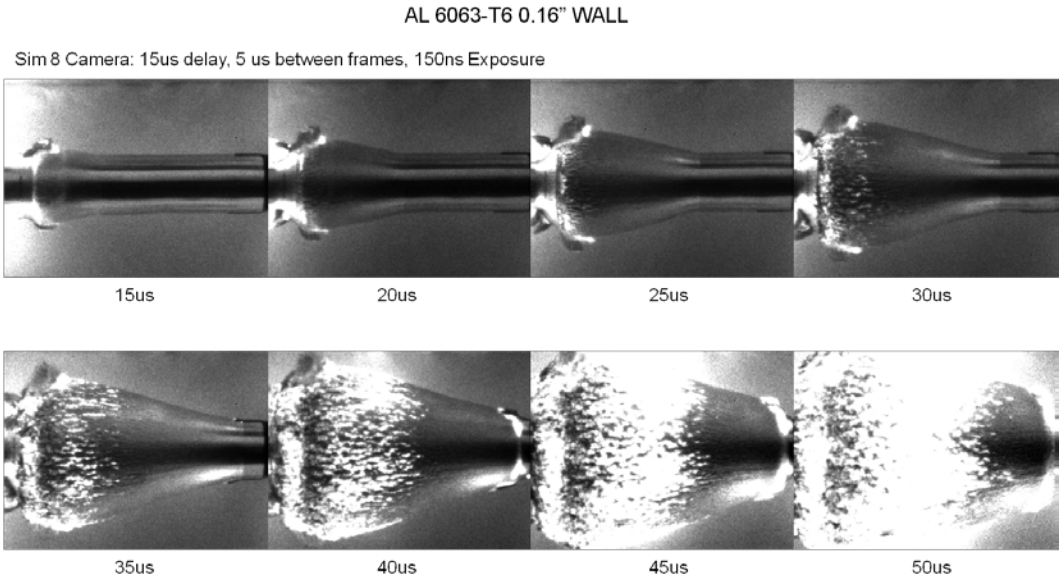

Fig. A-2 Experiment B

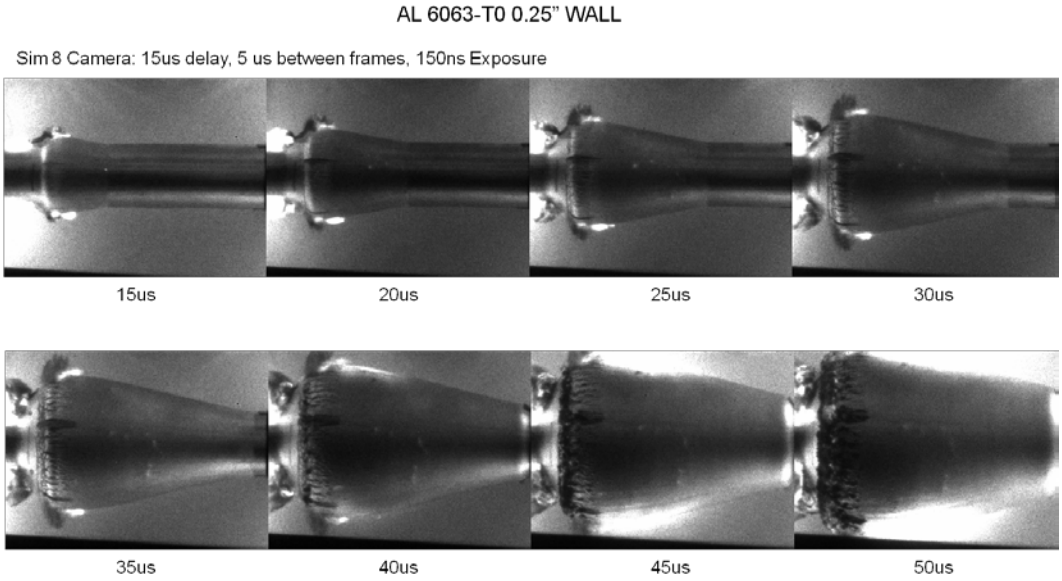

Fig. A-3 Experiment C

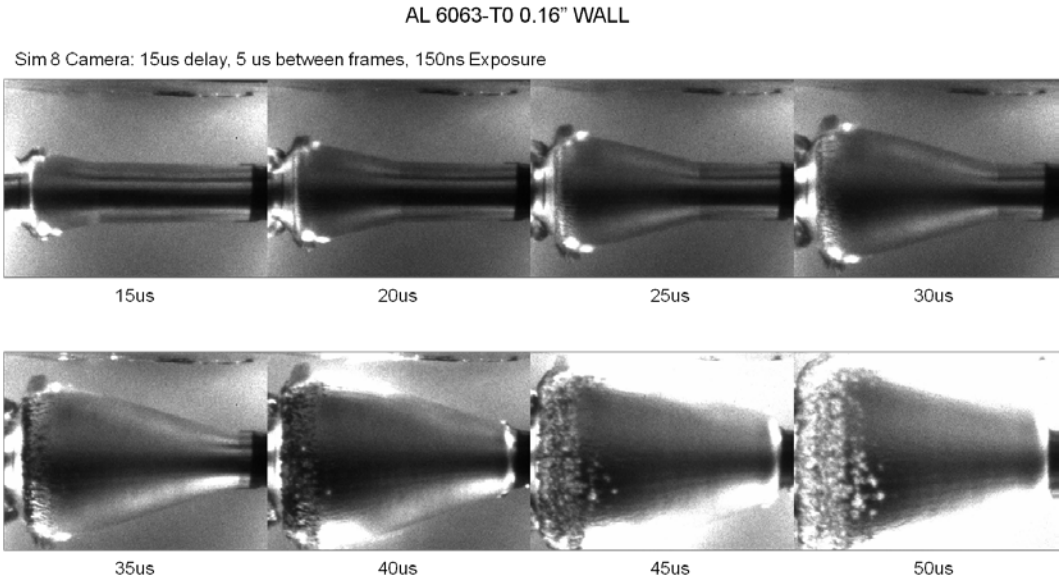

Fig. A-4 Experiment D

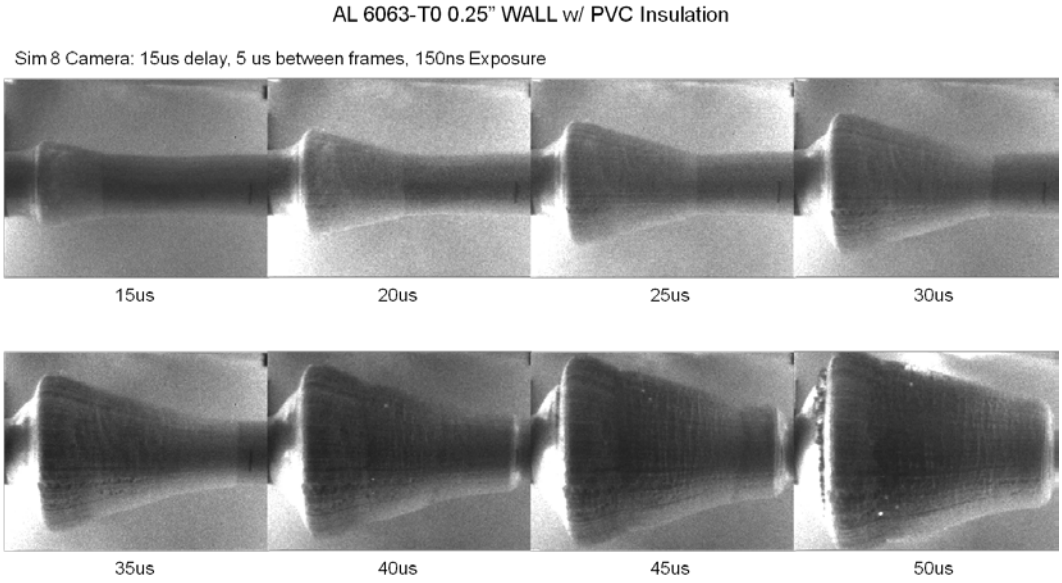

Fig. A-5 Experiment E

List of Symbols, Abbreviations, and Acronyms

Al	aluminum
ARL	US Army Research Laboratory
HP	high pressure
MFC	Magnetic Flux Compression
mm	millimeter(s)
PVC	polyvinyl chloride
SS	stainless steel
TO	O temper

1 (PDF) DEFENSE TECHNICAL INFORMATION CTR DTIC OCA

2 (PDF) DIRECTOR US ARMY RESEARCH LAB RDRL CIO L IMAL HRA MAIL & RECORDS MGMT

1 (PDF) GOVT PRINTG OFC A MALHOTRA

26 (PDF) DIR USARL RDRL WMP A C HUMMER S BILYK W UHLIG P BERNING M COPPINGER J CAZAMIAS RDRL WMP D S HALSEY A BARD M KEELE D KLEPONIS J RUNYEON D PETTY R DONEY G VUNNI RDRL WMP E P BARTKOWSKI S BARTUS M BURKINS D HACKBARTH T JONES C KRAUTHAUSER P SWOBODA RDRL WMP F N GNIAZDOWSKI RDRL WMP B C HOPPEL RDRL WMP D LYON RDRL SED P C TIPTON D PORSCHET

1 (PDF) US ATEC E SANDERSON

6 (PDF) US ARMY TACOM J WHITE L FRANKS D TEMPLETON M LAWSON J HITCHCOCK N COOPER

2 (PDF) PM ABCT J ROWE E BARSHAW

4 (PDF) NATL GROUND INTLLGNC CTR D EPPERLY T SHAVER T WATERBURY D DOBROWOLSKI

1 (PDF) PM MRAP J PEREZ (JPO)

1 (PDF) DARPA/DSO L CHRISTODOULOU

1 (PDF) PM BFVS D SPENCER

1 (PDF) NSWC CARDEROCK DIV R PETERSON

1 (PDF) SANDIA NATL LAB E STRACK

2 (PDF) LAWRENCE LIVERMORE NATL LAB A JOHNSON J SOLBERG

1 (PDF) LOS ALAMOS NATL LAB D REISMAN

2 (PDF) BAE SYSTEMS LANDS & ARMAMENTS R APPLETON J PERONA

2 (PDF) GDLS R NICOL M KAUTZER